

# THE FIRST RESULT OF THE NEUTRINO MAGNETIC MOMENT MEASUREMENT IN THE GEMMA EXPERIMENT.

A.G. Beda<sup>†</sup>, V.B. Brudanin<sup>†\*</sup>, E.V. Demidova<sup>†</sup>, V.G. Egorov<sup>‡</sup>, M.G. Gavrilov<sup>†</sup>, M.V. Shirchenko<sup>‡</sup>, A.S. Starostin<sup>†\*\*</sup>,  
Ts. Vyllov<sup>‡</sup>

<sup>†</sup> ITEP (State Science Center, Institute for Theoretical and Experimental Physics, Moscow, Russia)

<sup>‡</sup> JINR (Joint Institute for Nuclear Research, Dubna, Russia)

\* e-mail: Brudanin@nusun.jinr.ru

\*\* e-mail: Starostin@itep.ru

The first result of the neutrino magnetic moment measurement at the Kalininskaya Nuclear Power Plant (KNPP) with the GEMMA spectrometer is presented. An antineutrino-electron scattering is investigated. A high-purity germanium detector of 1.5 kg placed 13.9 m away from the 3 GW reactor core is used in the spectrometer. The antineutrino flux is  $2.73 \times 10^{13} \bar{\nu}_e/\text{cm}^2/\text{s}$ . The differential method is used to extract the  $\nu$ - $e$  electromagnetic scattering events. The scattered electron spectra taken in 6200 and 2064 hours for the reactor *on* and *off* periods are compared. The upper limit for the neutrino magnetic moment  $\mu_\nu < 5.8 \times 10^{-11} \mu_B$  at 90% CL is derived from the data processing.

## 1 Introduction

In recent years a series of remarkable indications of the atmospheric, solar and reactor neutrino oscillations have been observed. Analysis of the entire experimental data allows a conclusion that the neutrino has a finite mass and the neutrino state mixing process to be defined. However, some fundamental neutrino properties are not determined as yet. One of them is the neutrino magnetic moment (NMM). For the massive neutrino the Minimally Extended Standard Model predicts a very small NMM value which cannot be experimentally observed at present:

$$\mu_\nu = \frac{3 e G_F}{8 \pi^2 \sqrt{2}} \cdot m_\nu \approx 3 \cdot 10^{-19} \mu_B \cdot \frac{m_\nu}{1\text{eV}} \quad (1)$$

Here,  $\mu_B$  is the Bohr magneton ( $\mu_B = eh/2m_e$ ) and  $m_\nu$  is the neutrino mass. On the other hand, there is a number of extensions of the theory beyond the Minimal Standard Model where the NMM could be at a level of  $(10^{-12} \div 10^{-10}) \mu_B$  irrespective of the neutrino mass [1, 2, 3]. A rough upper limit of the NMM value can be obtained from the astrophysical considerations, namely from the parameters of some stars at the last stage of their evolution when energy is released mainly as a neutrino flux. In this case, estimation of the mass of the helium star core at the moment of the outburst, luminosity of White Dwarfs and the neutrino energy spectrum at the Supernova explosion provide the astrophysical NMM upper limits in the range of  $(10^{-12} \div 10^{-11}) \mu_B$  [4]. Note that these results are model dependent, and therefore it is rather important to make laboratory NMM measurements sensitive enough to reach the  $\sim 10^{-11} \mu_B$  region. It would allow one

to test a large variety of NMM hypotheses beyond the Standard Model.

The NMM measurements were started more than 30 years ago. They use reactor and solar (anti)neutrinos in laboratory experiments. The first paper [5] on the observation of  $\bar{\nu}$ - $e$  scattering was published in 1976. The experiment was carried out by Reines' group at the Savannah River laboratory. Later, in 1989 P. Vogel and J. Engel [6] derived the following upper limit for the NMM from these data:  $\mu_\nu < (2 \div 4) \times 10^{-10} \mu_B$ . In 1992 and 1993 the results of the reactor experiments performed at the Krasnoyarsk reactor by a group from the Kurchatov Institute [7] and at the Rovno reactor by a group from Gatchina [8] were published. Their NMM upper limits were  $2.4 \times 10^{-10} \mu_B$  and  $1.9 \times 10^{-10} \mu_B$ , respectively.

The recent reactor experiments have been carried out by the MUNU [9] and TEXONO [10] collaborations over the period 2001–2005. The MUNU NMM upper limit is  $\mu_\nu < 9.0 \times 10^{-11} \mu_B$ , whereas the TEXONO experiment produced the currently best limit:  $\mu_\nu < 7.2 \times 10^{-11} \mu_B$  (however, the method of the TEXONO data treatment and the result extraction seems to be questionable). Thus, over a period of thirty years the sensitivity of reactor experiments increased only by a factor 3.

The NMM upper limit comparable with the above reactor results was obtained by the SuperKamiokande collaboration [11] in the solar neutrino investigations. Analysis of the recoil electron spectrum after the solar neutrino scattering gives  $\mu_\nu < 1.1 \times 10^{-10} \mu_B$ . It should be mentioned that the NMM results in the reactor and Sun experiments may be different. Due to the oscillation process, the flavor composition of the initial neu-

trino flux changes during the propagation in vacuum as follows [12]:

$$|\nu_e(L)\rangle = \sum_k U_{ek} e^{-iE_\nu L} |\nu_k\rangle, \quad (2)$$

where  $E_\nu$  is the neutrino energy,  $L$  is the distance from the source,  $U_{ek}$  is the unitary mixing matrix element,  $k$  labels the mass eigenstates, and the subscript  $e$  labels the initial flavor. Simultaneously with the change of the neutrino flavor composition, the effective value of the NMM also changes:

$$\mu_\nu^2(E_\nu, L) = \sum_j \left| \sum_k U_{ek} e^{-iE_\nu L} \mu_{jk} \right|^2, \quad (3)$$

where the summations  $j, k$  are over the mass eigenstates,  $\mu_{jk}$  are the magnetic moments or constants that characterize the coupling of the neutrino mass eigenstates  $\nu_j$  and  $\nu_k$  to the electromagnetic field.

Above the flavour mixing in vacuum was considered. But in the case of solar neutrinos it must be modified for matter-enhanced oscillation (the resonant MSW effect). Because of this effect the solar neutrino flux at the Earth surface is a mixture of electron, muon and (possibly) tau neutrinos. Since the length of antineutrino propagation in the reactor experiments is rather short, the neutrino flux includes only electron antineutrinos. Thus, a comparison of the NMM measurements in the reactor and solar experiments can be highly productive [12, 13].

In this paper, the first results of the NMM measurement by the collaboration of the Institute for Theoretical and Experimental Physics (ITEP, Moscow) and the Joint Institute for Nuclear Research (JINR, Dubna) are presented. The measurements are carried out with the *GEMMA* spectrometer (Germanium Experiment on measurement of Magnetic Moment of Antineutrino) at the 3 GW reactor of the Kalininskaya Nuclear Power Plant (KNPP).

## 2 Experimental approach

A laboratory measurement of the NMM is based on its contribution to the  $\nu$ - $e$  scattering. For the nonzero NMM the  $\nu$ - $e$  differential cross section is given [6] by the sum of the standard *weak* interaction cross section ( $d\sigma_W/dT$ ) and the *electromagnetic* one ( $d\sigma_{EM}/dT$ ):

$$\frac{d\sigma_W}{dT} = \frac{G_F^2 m_e}{2\pi} \left[ \left(1 - \frac{T}{E_\nu}\right)^2 (1 + 2 \sin^2 \theta_W)^2 + 4 \sin^2 \theta_W - 2 \left(1 + 2 \sin^2 \theta_W\right) \sin^2 \theta_W \frac{m_e T}{E_\nu^2} \right], \quad (4)$$

$$\frac{d\sigma_{EM}}{dT} = \pi r_0^2 \cdot \left(\frac{\mu_\nu}{\mu_B}\right)^2 \cdot \left(\frac{1}{T} - \frac{1}{E_\nu}\right), \quad (5)$$

where  $E_\nu$  is the incident neutrino energy,  $T$  is the electron recoil energy,  $r_0$  is the electron radius ( $\pi r_0^2 = 2.495 \times 10^{-25} \text{ cm}^2$ ) and  $\theta_W$  is the Weinberg angle.

In the reactor experiments the pressurized water nuclear reactors (PWR) of  $\sim 3$  GW thermal power are used as strong sources of antineutrinos. In this case one measures the energy spectrum of electron recoil caused by both weak (W) and electromagnetic (EM) scattering of the neutrinos, i.e. the sum of these processes, so that EM plays the role of unremovable background correlated with the reactor operation. Figure 1 shows the

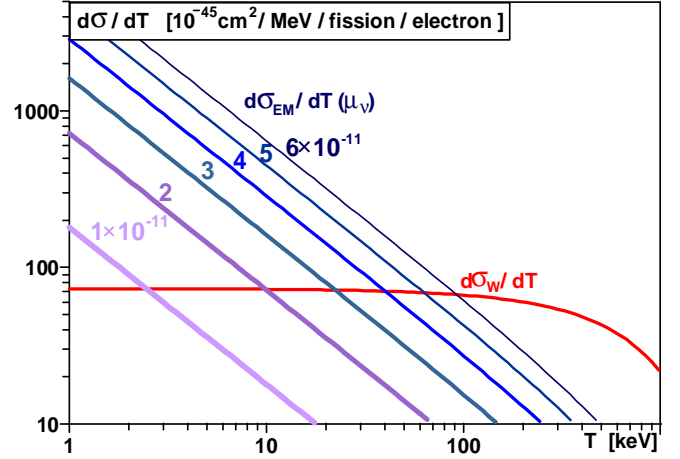


Figure 1: Weak (W) and electromagnetic (EM) cross-sections calculated for several NMM values.

differential cross sections (4) and (5) averaged over the typical antineutrino reactor spectrum vs the electron recoil energy. One can see two important features in this figure. First, because of an extremely low cross section, the problem of the signal-to-background ratio arises, which in its turn requires strong suppression of all background components. Second, at low recoil energy ( $T \ll E_\nu$ ) the value of  $d\sigma_W/dT$  becomes constant, while  $d\sigma_{EM}/dT$  increases as  $T^{-1}$ , so that lowering of the detector threshold leads to the considerable increase of the NMM effect with respect to the weak contribution.

More than fifteen years ago M.B.Voloshin and A.S. Starostin (ITEP) proposed to search for NMM by means of a low-background germanium spectrometer (LBGS) similar to ones used in the  $\beta\beta$ -decay experiments [14] with  $^{76}\text{Ge}$ . The idea was realized within the project GEMMA by the ITEP-JINR collaboration in 1997 when the single-crystal Ge(Li) LBGS was constructed and tested [15]. The LBGS has a low level of intrinsic noise and additional background suppression in the energy range below 100 keV due to absorption of the low energy component of the external radiation by dead layers of the germanium detector (GD). A combination of these advantages allows measurements in the energy range  $\sim (2 - 100)$  keV. In addition, the LBGS has a number of characteristics which open the way to reaching an ultralow level of radiation background [16]. Radioactive impurities in the germanium crystal do not exceed  $10^{-14}$  g/g, that is 5–7 orders of magnitude lower than in pure metals. Due to a small size of the GD it

can be easily shielded with such rare and expensive materials as oxygen-free electrolytic copper, archaeological lead free of radioactive  $^{210}\text{Pb}$ , etc. One can use NaI crystals as an active shielding against the charged component of cosmic radiation and for suppression of the Compton component of external radiative background.

### 3 The GEMMA Spectrometer

The basic challenge of the experiment is to decrease the background level of the surface (not *underground!*) setup, placed close to the reactor, down to the value of (1–2) events/keV/kg/day. During development of the spectrometer many different approaches were analyzed in order to solve this problem [15]. Spectrometers with passive shielding and those with active shielding were considered. The latter approach was adopted since it provides better suppression of all background components under strong cosmic radiation and operation of the nuclear reactor. The detailed description of the GEMMA spectrometer tested under the ITEP laboratory conditions is given in [15, 17]. Two important changes were made later during the assembling of the spectrometer under the KNPP reactor. Firstly, the four-crystal Ge(Li) detector was replaced by a one-crystal high-purity germanium detector (HPGe) of 1.5 kg in mass. Secondly, we abandoned neutron shielding in the form of two 8-cm-thick layers of borated polyethylene, since neutron background under the reactor was found to be substantially lower than in the surface laboratory. Besides, removing 16 cm of polyethylene, we made the spectrometer more compact and thus could increase the lead shielding against external  $\gamma$ -radiation.

We use standard CAMAC and NIM modules in the electronic data acquisition system. The analog part operates in the following way. The HPGe preamplifier signals (Fig. 2) are distributed among five spectroscopic amplifiers. Three of them have the same gain, but different shaping times ( $\tau_1=2\mu\text{s}$ ,  $\tau_2=4\mu\text{s}$ ,  $\tau_3=12\mu\text{s}$ ) and take data in the 380 keV energy range. The fourth channel is used for the spectrum monitoring in the range up to 2.8 MeV. External gates for the corresponding ADCs are produced by a special peak-sensitive discriminator connected to a logarithmic amplifier ( $\tau_0 = 1\mu\text{s}$ ). It was found that such a trigger system provides better linearity in the wide energy range (1.5 ÷ 2800) keV.

The use of three amplifiers with different shaping time makes it possible to suppress low-frequency (LF) and high-frequency (HF) circuit noises. The first one can be induced by 50-Hz power supply, as well as microphonics: environmental acoustic noise, bubbling of liquid nitrogen in the Dewar vessel affecting the detector cryostat, vibrations in the surrounding equipment,

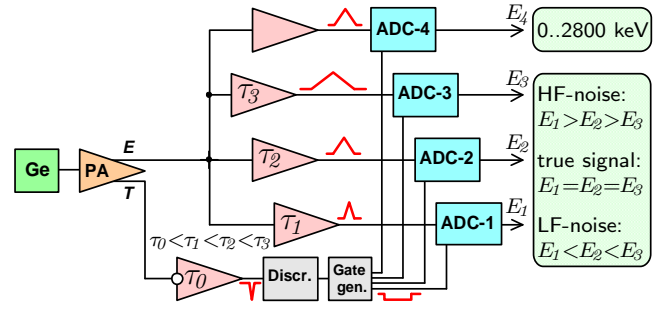


Figure 2: Analog part of the data acquisition system.

etc. The sources of the HF circuit noises include pulse radiofrequency interference due to operation of the PC and electronic units, fluctuations of the detector dark current, thermal noise of the preamplifier FET. The LF and HF noise signals are amplified in different ways for different bands ( $\tau_1 < \tau_2 < \tau_3$ ). The relation  $E_1 = E_2 = E_3$  is valid for true signals and distorted for noise signals, which allows their discrimination [18].

### 4 Preparation work

The GEMMA spectrometer is installed under the second reactor block of the KNPP. Before the installation, we measured the background caused by  $\gamma$ -radiation, thermal neutrons, charged component of cosmic radiation and radioactive aerosol pollution. The  $\gamma$ -radiation background was measured with a portable germanium detector. An integral level of the radiation background was an order of magnitude higher than usually indoors, and it was caused mainly by long-lived fission products:  $^{134,137}\text{Cs}$  and  $^{60}\text{Co}$ . The measurements were repeated several times during the reactor ON and reactor OFF periods. The radiation background level was the same within the statistical errors in both periods. As a result, it was decided that the existing shielding (15 cm of Pb + 5 cm of Cu + 14 cm of NaI) is quite enough to suppress the external  $\gamma$ -background.

The charged component of cosmic rays (muons) was detected with two coincident plastic scintillator counters of size  $120 \times 120 \times 4 \text{ cm}^3$ . The absolute value and the angular distribution of the muon flux were measured. Compared to the surface laboratory conditions, the muon flux was found to be reduced by a factor of 6 due to passive shielding by the building structure and the reactor itself. At the same time, the factor of muon flux suppression was 10 at the angles of  $\pm 20^\circ$  with respect to the vertical<sup>1</sup> and only 3 at the angles of  $70^\circ \div 80^\circ$ , which corresponds to 70 and 20 meters of water equiv-

<sup>1</sup>In more details, the angular distribution of cosmic muons was considered, for instance, in [19].

alent, resp. The above passive shielding completely eliminates the hadronic component of the primary cosmic rays.

Neutrons were detected with a set of proportional  $^3\text{He}$  counters enclosed in a polyethylene moderator. The measurements were relative: the neutron flux at the spectrometer site was compared to the flux at the surface laboratory. At the surface one can normally observe secondary atmospheric neutrons and tertiary neutrons due to muon capture, the fraction of the tertiary neutrons being  $(10\div 20)\%$  [20] or about 160 n/g/year. Fast secondary and tertiary neutrons can be detected after their thermalization in the moderator. At the spectrometer site the secondary neutrons must be absent because of the upper passive shielding. The tertiary neutron contribution must decrease in proportion to the muon flux (by a factor of 6), but some additional neutrons can originate from the reactor core. The measurements proved that the neutron flux at the spectrometer site is reduced by a factor of 30 compared to the surface. These results correspond to the above muon measurements and indicate that the reactor neutrons are not significant.

Much attention was paid to the contamination of the experimental room with a radioactive dust since the background level could significantly increase if radioactive dust get settled inside the shielding during the setup assembling. Samples were taken in different places of experimental room beneath the reactor and investigated with the GEMMA spectrometer in the ITEP low-background laboratory. Radioactive nuclides were identified and their activity was measured. In addition, different methods of decontamination were investigated. As a result of these investigations, it was decided to cover the floor with special plastic. Once this work was done, test measurements were carried out, and it became clear that radioactive dust contamination was significantly reduced.

## 5 Reactor antineutrinos

The setup is located under the 3-GW PWR at a distance of 13.9 m from the center of the reactor core. During the measurements at the KNPP the energy threshold of GEMMA spectrometer was 2.5 keV. At such a low threshold the recoil electron spectrum does not depend on details of the reactor antineutrino spectrum and is determined by the *total* reactor antineutrino flux  $\Phi_\nu$ :

$$\Phi_\nu = N_f N_\nu / 4\pi R^2, \quad (6)$$

where  $N_f$  is the number of fissions in the reactor core per second,  $N_\nu$  is the antineutrino yield per fission,  $R$  is the distance from the center of the reactor core.  $N_f$  can be expressed in terms of the reactor thermal power  $W$  and an average energy  $E_f$  per fission:

$$N_f = W/E_f. \quad (7)$$

The energy  $E_f$  depends on the reactor type, fuel composition and time elapsed since the beginning of the reactor cycle. At the beginning of the one-year reactor cycle the typical fuel composition is the following[21]:

$$\begin{aligned} {}^{235}\text{U} : \quad \alpha_5(t=0) &= 69\% \\ {}^{239}\text{Pu} : \quad \alpha_9(t=0) &= 21\% \\ {}^{238}\text{U} : \quad \alpha_8(t=0) &= 7\% \\ {}^{241}\text{Pu} : \quad \alpha_1(t=0) &= 3\% \end{aligned} \quad (8)$$

As  ${}^{235}\text{U}$  burns down, the plutonium fissile isotopes  ${}^{239}\text{Pu}$  and  ${}^{241}\text{Pu}$  are produced in the reactor core. The following fuel composition is considered as "standard":

$$\begin{aligned} {}^{235}\text{U} : \quad \alpha_5 &= 58\% \\ {}^{239}\text{Pu} : \quad \alpha_9 &= 30\% \\ {}^{238}\text{U} : \quad \alpha_8 &= 7\% \\ {}^{241}\text{Pu} : \quad \alpha_1 &= 5\% \end{aligned} \quad (9)$$

and the corresponding energies  $E_{fk}$  are:

$$\begin{aligned} {}^{235}\text{U} : \quad E_{f5} &= 201.9 \text{ MeV / fission} \\ {}^{239}\text{Pu} : \quad E_{f9} &= 210.0 \text{ MeV / fission} \\ {}^{238}\text{U} : \quad E_{f8} &= 205.5 \text{ MeV / fission} \\ {}^{241}\text{Pu} : \quad E_{f1} &= 213.6 \text{ MeV / fission} \end{aligned} \quad (10)$$

The average  $E_f$  value is

$$E_f = \sum_k \alpha_k E_{fk} = 205.3 \text{ MeV / fission}. \quad (11)$$

From (7)–(11) one can get the following  $N_f$  value for the 3 GW power:

$$N_f(3 \text{ GW}) = 9.14 \times 10^{19} \text{ fissions / s}. \quad (12)$$

The antineutrino yield per fission  $N_\nu$  can be represented as a sum of two components

$$N_\nu = N^F + N^C, \quad (13)$$

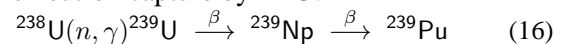
where  $N^F$  corresponds to the antineutrinos produced in  $\beta$ -decay of the  ${}^{235}\text{U}$ ,  ${}^{239}\text{Pu}$ ,  ${}^{238}\text{U}$  and  ${}^{241}\text{Pu}$  fission products. These values were calculated several times, the results being in agreement to  $\sim 1\%$ . Averaging over three works [22]–[24], we get

$$\begin{aligned} {}^{235}\text{U} : \quad N_{235}^F &= 6.12 \bar{\nu}_e / \text{fission} \\ {}^{239}\text{Pu} : \quad N_{239}^F &= 5.53 \bar{\nu}_e / \text{fission} \\ {}^{238}\text{U} : \quad N_{238}^F &= 7.11 \bar{\nu}_e / \text{fission} \\ {}^{241}\text{Pu} : \quad N_{241}^F &= 6.36 \bar{\nu}_e / \text{fission} \end{aligned} \quad (14)$$

and the final value is

$$N^F = \sum_k \alpha_k N_k^F = 6.0 \bar{\nu}_e / \text{fission}. \quad (15)$$

The second component  $N^C$  corresponds to the antineutrinos emitted in  $\beta$ -decay of the nuclides produced due to the neutron capture by  ${}^{238}\text{U}$ :



The value of  $N^C$  equals to 1.2 and was first derived in [25] with a precision of 5%. Finally, for the total number of antineutrinos per fission  $N_\nu$  we get 7.2, and substitution of the  $N_\nu$  and  $N_f$  values into (6) gives the following antineutrino flux at the GEMMA site:

$$\Phi_\nu = 2.73 \times 10^{13} \bar{\nu}_e / \text{cm}^2 / \text{s}. \quad (17)$$

## 6 The measurement and preliminary data processing

In order to get a recoil electron spectrum, we used a difference method comparing the spectra measured at the reactor operation (ON) and shut-down (OFF) periods. In this work we consider  $\sim 1$  year measurement from 15.08.2005 to 20.09.2006, including 6200 and 2064 hours of the reactor ON and OFF periods<sup>2</sup>, respectively.

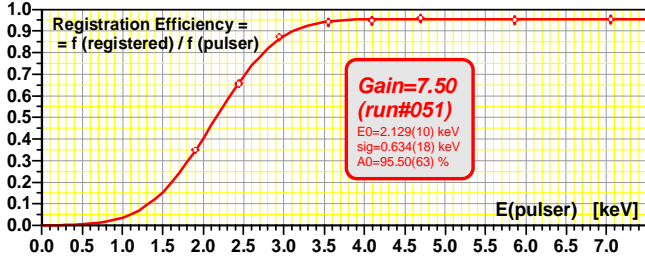


Figure 3: Detection efficiency measured with a pulser.

During the measurements, the signals of the HPGe detector, anti-compton NaI shielding and outer anti-cosmic plastic counters were collected. The energy threshold of the "hard" trigger (*Discriminator* in Fig. 2) was as low as 1.5 keV. Detection efficiency just above the threshold was checked with a pulser (Fig. 3). The neutrino flux monitoring in the ON period was done via the reactor thermal power measured with the 0.7% accuracy. The setup was in continuous operation during all the period mentioned above. Some loss of the measurement time was caused by occasional failures of the acquisition electronics, regular liquid nitrogen filling (increasing the microphonic noise) and sporadic appearance of additional  $\gamma$ -background, mainly from  $^{133}\text{Xe}$  ( $E_\gamma = 81$  keV) and  $^{135}\text{Xe}$  ( $E_\gamma = 250$  keV), due to a failure of the setup gas tightness. Finally, the data processing was based on 5184 hours (reactor ON) and 1853 hours (reactor OF).

The data processing starts with identification and subsequent rejection of background events. At the same time, the efficiency of all the passive and active shielding components was analyzed. The main effect of the external radiation background suppression was achieved due to combined passive shielding (PS). The factor of background suppression in the energy range from 2 keV up to 200 keV exceeded four orders of magnitude. A veto produced by the inner and outer active shielding signals (NaI and plastic counters) provides background suppression by one more order of magnitude (Fig. 4).

In order to reduce the microphonic and electronic circuit noise, the simplest Fourier analysis was used. To

<sup>2</sup>The OFF period includes the time for the planned replacement of the fuel elements, as well as the unplanned reactor shutdowns caused by other reasons.

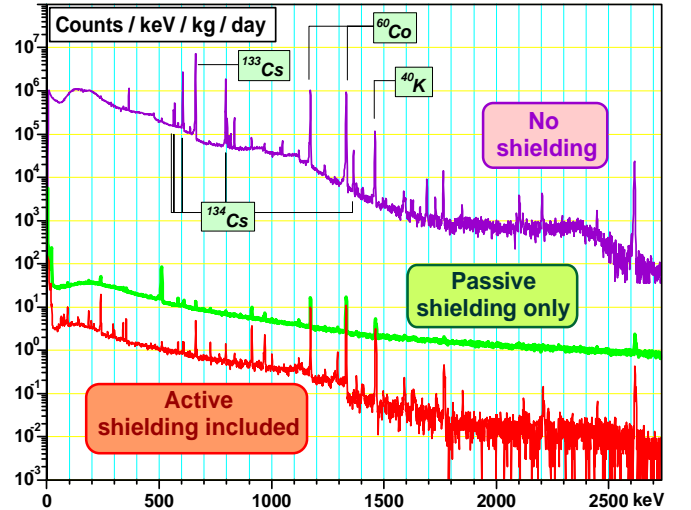


Figure 4: Background suppression with shielding.

compare the pulse heights from three amplifiers (Fig. 2), three 2D plots are built: ( $E_1$  vs  $E_2$ ), ( $E_2$  vs  $E_3$ ) and ( $E_3$  vs  $E_1$ ). An example of such a plot is shown in Fig. 5.

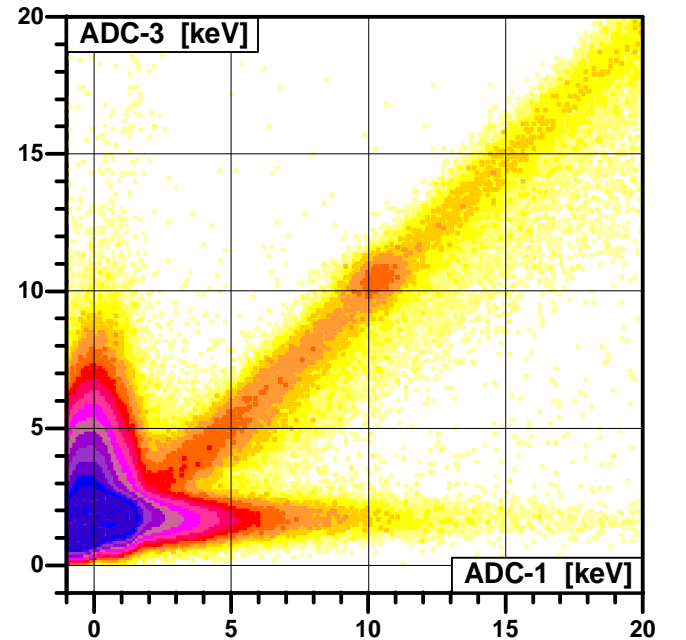


Figure 5: Example of the Fourier analysis.

All true events fall into a diagonal (within the energy resolution), whereas the events caused by microphonic and electronic noise are distributed in a different way. The result of circuit noise suppression with the Fourier analysis is presented in Fig. 6. It can be seen that the actual energy threshold can be decreased down to 3 keV.

After the selection of true signals, ON and OFF energy spectra normalized to the measurement live time were constructed. The normalization takes into account the PC dead time (normally less than 1%) and random coincidences with the veto signals (about 4%). The statistics loss caused by the Fourier analysis ( $< 1\%$ ) was

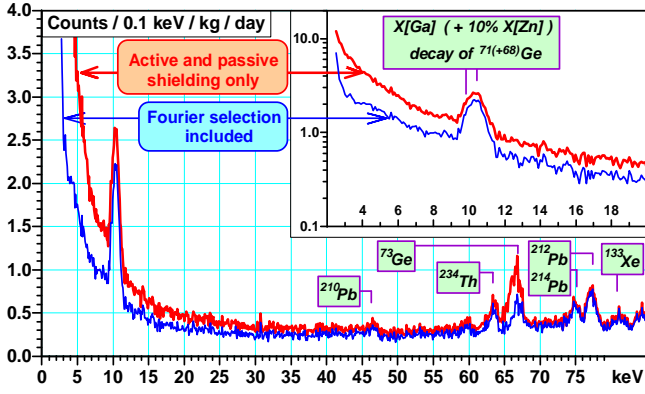


Figure 6: Noise suppression with the Fourier analysis.

estimated from the difference of the background  $\gamma$ -line intensities.

Energy spectra shown in Figs. 4 and 6 give an idea of the background level and its origin. As is seen from the figures, the count rate in the energy range from 30 to 45 keV was  $\sim 2$  events/keV/kg/day. Table 1 shows the most intense  $\gamma$ -lines measured with the GEMMA spectrometer at the ITEP laboratory and at the KNPP.

Most of the  $\gamma$ -lines originate from long lived fission products ( $^{137}\text{Cs}$ ,  $^{134}\text{Cs}$ ,  $^{60}\text{Co}$ ), natural  $^{238}\text{U}$  and  $^{232}\text{Th}$  chains, and  $^{40}\text{K}$ . One can see that the U-chain background ( $^{214}\text{Bi}$  and  $^{214}\text{Pb}$  lines) at the ITEP and KNPP is the same, whereas the Th-chain and  $^{40}\text{K}$  background is higher at KNPP. It can be explained by the contamination of the cryostat components in the process of replacing Ge(Li) detector by the HPGe detector before the beginning of the measurements. The presence of  $^{60}\text{Co}$  and  $^{137}\text{Cs}$   $\gamma$ -lines in the KNPP spectrum is caused by the spectrometer contamination during the setup assembling at the KNPP.

Several  $\gamma$ -lines originate from the Ge detector activation by thermal neutrons producing  $^{75}\text{Ge}$ ,  $^{77m}\text{Ge}$  and  $^{77}\text{As}$   $\beta$ -active isotopes. A neutron shielding of borated polyethylene was not used in KNPP measurements. In spite of this fact, the neutron-induced background there was even lower than at the ITEP laboratory. The estimated contribution of the thermal neutrons to the background was about 2%.

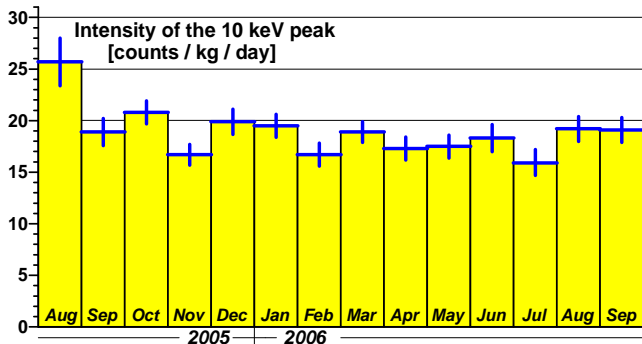
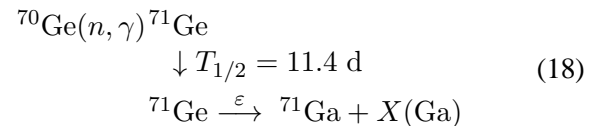


Figure 7: Time evolution of the 10 keV peak.

Energy [ keV ]	Origin of the line	Intensity [ cnts / kg / day ]	
		@ KNPP	@ ITEP
10.37 10.30	$^{70}\text{Ge}(n,\gamma)^{71}\text{Ge}$ , 11.4 d $^{70}\text{Ge}(n,3n)^{68}\text{Ge}$ , 271 d	17.5±0.4	—
46.50	$^{210}\text{Pb}$		
63.30	$^{234}\text{Pa}$	3.5±0.2	—
66.70	$^{72}\text{Ge}(n,\gamma)^{73m}\text{Ge}$	4.5±0.2	5.5±1.5
74.80	$^{214}\text{Pb}$	2.8±0.1	5.3±1.9
77.10	$^{214}\text{Pb}$	5.4±0.2	7.1±1.9
92.60	$^{234}\text{Pa}$	11.8±0.3	—
139.90	$^{74}\text{Ge}(n,\gamma)^{75m}\text{Ge}$	3.4±0.2	5.0±2.0
186.20	$^{226}\text{Ra}$	9.0±0.3	2.1±0.5
198.30	$^{70}\text{Ge}(n,\gamma)^{71m}\text{Ge}$	2.3±0.2	3.5±1.2
238.60	$^{212}\text{Pb}$	29.4±0.5	7.5±1.6
295.20	$^{214}\text{Pb}$	4.4±0.2	5.7±1.1
338.30	$^{228}\text{Ac}$	4.7±0.2	—
351.90	$^{214}\text{Pb}$	8.0±0.3	7.5±0.9
511.00	Annihilation	1.0±0.1	2.5±1.0
583.20	$^{208}\text{Tl}$	1.7±0.1	—
604.70	$^{134}\text{Cs}$	1.6±0.1	—
609.30	$^{214}\text{Bi}$	2.4±0.1	2.5±0.9
661.66	$^{137}\text{Cs}$	8.5±0.3	—
727.30	$^{212}\text{Bi}$	2.2±0.1	—
911.10	$^{228}\text{Ac}$	8.4±0.3	$\leq 1.0$
969.00	$^{228}\text{Ac}$	4.7±0.2	—
1173.20	$^{60}\text{Co}$	25.7±0.5	—
1332.50	$^{60}\text{Co}$	30.2±0.5	—
1460.80	$^{40}\text{K}$	13.4±0.1	4.1±0.5
1764.50	$^{214}\text{Bi}$	2.1±0.1	1.8±0.3
2614.50	$^{208}\text{Tl}$	1.8±0.1	0.4±0.1

Table 1: Gamma-lines

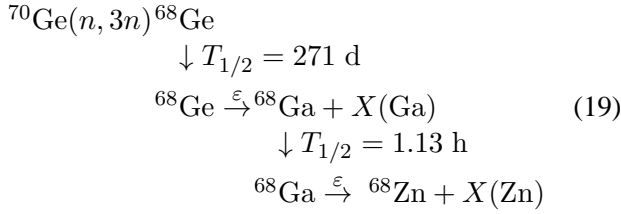
The  $\gamma$ -line at 10.37 keV can be due to the germanium detector activation by both thermal and fast cosmogenic neutrons. In the former case it is due to the  $(n,\gamma)$  reaction followed by  $\epsilon$  capture



emitting an Auger and/or X-ray cascade with the total energy deposit of 10.367 keV.

In the latter case it is caused by the  $(n,3n)$  reaction and is accompanied with a weak 9.659-keV line from

the decay of the granddaughter  $^{68}\text{Ga}$  nucleus:



Branching of the second  $\varepsilon$  capture is only about 10%, so that a slightly broadened peak with a mean energy of 10.30 keV should be observed.

Since the intensity of this  $\gamma$ -line (Fig. 7) was almost constant throughout the whole measurement period, it is believed that the first case (18) dominates over the second one (19).

## 7 The data processing

At low electron recoil energy the differential cross sections (4, 5) take an asymptotic form:

$$\frac{d\sigma_W}{dT} = 1.06 \times 10^{-44} \text{ cm}^2/\text{MeV} \quad (20)$$

$$\frac{d\sigma_{EM}}{dT} = \frac{2.495}{T} \cdot X \times 10^{-45} \text{ cm}^2/\text{MeV} \quad (21)$$

where the parameter  $X$  stands for the NMM squared in terms of  $10^{-10}$  Bohr magnetons:

$$X \equiv \left( \frac{\mu_\nu}{10^{-10} \mu_B} \right)^2. \quad (22)$$

To convert the cross sections  $d\sigma_{W,EM}/dT$  into the recoil electron spectra  $S_{W,EM}(T)$ , one has to multiply (20, 21) by a luminosity  $L$  which depends on the experimental conditions:

$$L = N_e \cdot \Phi_\nu, \quad (23)$$

where  $N_e = 4.0 \times 10^{26}$  is the number of electrons in the fiducial volume of the germanium detector and the neutrino flux  $\Phi_\nu$  is given by (17).

At low recoil energy one must take into account the atomic electron binding effects [25]. The energy  $q$  transferred to an electron in the antineutrino inelastic scattering (both weak and electromagnetic) on the  $i$ -subshell is

$$q = \varepsilon_i + T \quad (24)$$

where  $\varepsilon_i$  is the binding energy of the  $i$ -subshell [26], and  $T$  is the kinetic energy of the recoil electron. If the energy transfer is less than the binding energy ( $q < \varepsilon_i$ ), the electron cannot leave the subshell and be detected

via the ionization mode [27]. Formally, the spectrum must be corrected [28] by a function  $R$  (Fig. 8):

$$R(q) = \frac{1}{Z} \cdot \sum_i n_i \cdot \theta(q - \varepsilon_i), \quad (25)$$

where  $Z = 32$  for germanium,  $n_i$  is the number of electrons at the  $i$ -subshell, and the  $\theta$  factor is

$$\theta(q - \varepsilon_i) = \begin{cases} 1 & \text{if } q > \varepsilon_i \\ 0 & \text{if } q \leq \varepsilon_i \end{cases} \quad (26)$$

After the correction, the recoil energy spectra become as follows:

$$\begin{aligned}
 S_{EM}(T) &= \frac{d\sigma_{EM}}{dT} \cdot R \cdot L \\
 S_W(T) &= \frac{d\sigma_W}{dT} \cdot R \cdot L
 \end{aligned} \quad (27)$$

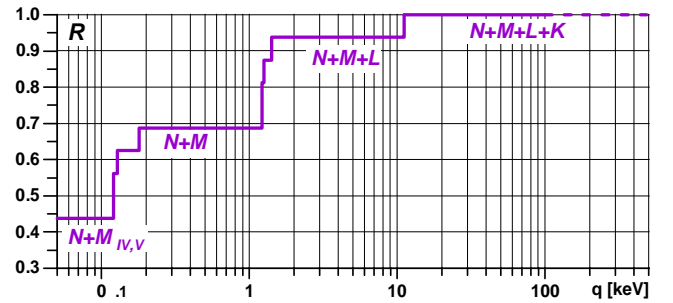


Figure 8: Correction for the electron binding energy.

As is seen in Fig. 8, the elastic and inelastic spectra are the same if the transferred energy exceeds the electron binding energy at the K-shell. The correction for bound electron states in the energy range from 11.1 keV down to the energy threshold (1.5 keV) comes to only 6.25%.

The data taken in the reactor ON period include two additional items ( $S_W$  and  $S_{EM}$ ) compared to the data taken in the reactor OFF period (*the other conditions being equal*):

$$S_{ON}(T) = S_{OFF}(T) + S_W(T) + S_{EM}(T, X) \quad (28)$$

In view of (20,21) and (27), an experimental estimate of the NMM can be extracted for any  $T$ -value:

$$X = \frac{(S_{ON} - S_{OFF} - S_W) \cdot T}{2.495 \times 10^{-45} \cdot R \cdot L}. \quad (29)$$

In this work, data were processed in the energy region of interest (ROI) from 3.0 keV to 61.3 keV with a step of 0.1 keV. To exclude 10.37-keV and 46.5-keV peaks, the above range was divided into three intervals: (3.0–9.2) keV, (11.2–44.0) keV and (48.0–61.3) keV (Fig. 9). Thus, with the given channel width of 0.1 keV, we get a set of 526 values of  $X_i \pm \Delta X_i$ , where  $i=[30..92, 112..440, 480..613]$  is the channel number

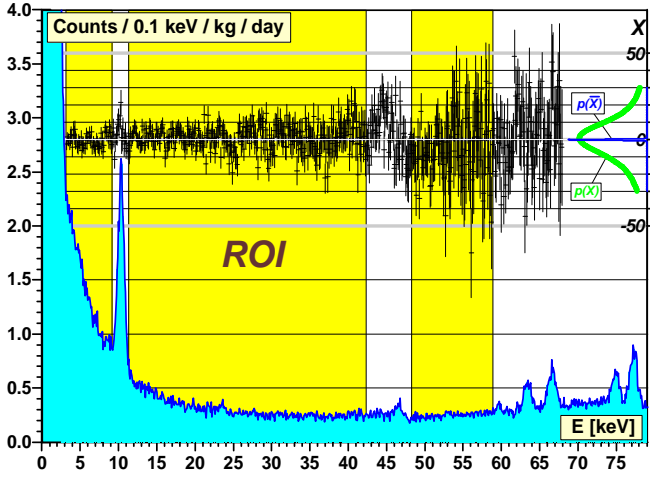


Figure 9: Extraction of  $X$  from the experimental ROI.

and  $\Delta X_i$  is the statistical error in each channel (the upper part of Fig. 9).

Distribution of  $X_i$  is shown in the right part of Fig. 9 as  $p(X)$ . It is a sum of 526 Gaussians with centers at  $X_i$  and variances  $\Delta X_i$ . The  $p(X)$  curve has a symmetrical Gaussian-like form, which proves the absence of systematic deviations. A product of these 526 Gaussians represents the distribution of the probabilistic estimation of the  $X$  mean value ( $p\langle X \rangle$ ); it is shown in Fig. 10. The distribution center falls below zero, in the unphysical region. According to the Bayes strategy recommended by the Particle Data Group [29], we renormalize this distribution in such a way that the area under the physical part of the curve is equal to 1. The integral of this part of the distribution is shown as a Confidence Level (CL) in Fig. 10 with a red solid line (dashed red line is an example of the result extraction at the 90% CL).

The systematic uncertainty of the result originates from several sources. The uncertainty of the reactor

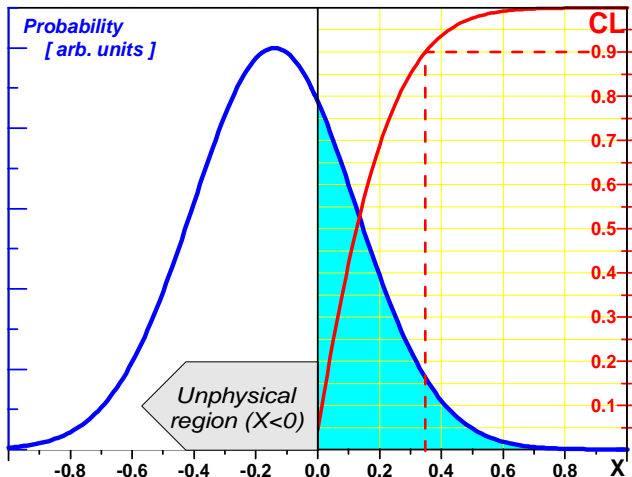


Figure 10: Estimation of the  $X$  mean value: probability (blue) and confidence level (red).

thermal power for PWR-1000 is about 0.7%. Another 3% uncertainty comes from the calculated value of the antineutrino flux  $\Phi_{\bar{\nu}}$ , which, in its turn, arises from the uncertainty of the reactor antineutrino spectrum. Then one must take into account the rejection efficiency and the efficiency of the Fourier analysis described above; they affect the final result indirectly, through the intensity of the ON and OFF spectra, and therefore have been included into the error bars of Fig. 9. Systematic uncertainties and the total systematic error are presented in Table 2.

Uncertainty source	$\Delta X/X$	$\Delta X$
Reactor thermal power	0.7%	$< 0.003$
Calculation of $\Phi_{\bar{\nu}}$ (ON)	3.0%	$< 0.015$
$\Phi_{\bar{\nu}}$ during the ON $\leftrightarrow$ OFF transitions	4.0%	$< 0.020$
Correction for the dead+vetoed time		$< 0.010$
Correction for the Fourier rejection		$< 0.020$
Total systematic error		$< 0.035$

Table 2: Systematic uncertainties

Considering the statistic and systematic errors, the following limit was derived for  $\mu_{\nu}$ :

$$\mu_{\nu} < 5.8 \times 10^{-11} \mu_B \quad (90\%CL). \quad (30)$$

Now the measurement is still in progress, and we expect to improve the GEMMA sensitivity to the NMM.

## 8 Conclusion

The first result on the neutrino magnetic moment measurement at the Kalininskaya Nuclear Power Plant (KNPP) obtained by the collaboration of ITEP (Moscow) and JINR (Dubna) with the GEMMA spectrometer is presented. The basis of the spectrometer is a high-purity germanium detector of 1.5 kg placed at the distance of  $\sim 13.9$  m from the center of the 3 GW WPR and surrounded with NaI active shielding, combined Pb+Cu passive shielding and muon veto plastic scintillators. The antineutrino flux at the spectrometer site is  $2.73 \times 10^{13} \bar{\nu}_e/\text{cm}^2/\text{s}$ . The data were taken during the operation of reactor (ON period = 6200 hours) and the reactor shutdown (OFF period = 2064 hours) from 15.08.05 to 20.09.06. When processing the recoil electron spectra caused by the electromagnetic and weak interactions, we took into account the effects of the electron binding in the germanium atoms. The limit on the neutrino magnetic moment of  $\mu_{\nu} < 5.8 \times 10^{-11} \mu_B$  at 90%CL was derived from the data analysis.

At present, the data taking is in progress. Simultaneously, we are preparing the experiment GEMMA II. Within the framework of this project we plan to use the



antineutrino flux of  $\sim 5.4 \times 10^{13} \bar{\nu}_e/\text{cm}^2/\text{s}$ , to increase the mass of germanium detector by a factor of four and to decrease the background level. These measures will provide the possibility of achieving the NMM limit at the level of  $1.5 \times 10^{-11} \mu\text{B}$ .

## 9 Acknowledgments

The authors thank Directorates of ITEP and JINR for constant support of this work. The authors are grateful to the administration of the KNPP and the staff of the KNPP Radiation Safety Department for permanent assistance in the experiment. We thank A.V. Salamatin for development of some electronic units and for participation in the background measurements.

This work is supported by the Russian Federal Agency of Atomic Energy and by the RFBR project No. 06-02-16281.

## REFERENCES

- [1] M.B. Voloshin, M.I. Vysotsky and L.B. Okun, *JETP (Rus.)* **64** (1986) 446.
- [2] M. Fukugita and T. Yanagida, *Phys. Rev. Lett.* **58** (1987) 1807.
- [3] S. Pakvasa and J.W.F. Valle, "Neutrino Properties Before and After KamLAND," **hep-ph/0301061**.
- [4] G.G. Raffelt, *Phys. Rep.* **320** (1999) 319; M. Fukugita, "Neutrinos in Cosmology and Astrophysics", preprint Yukawa Institute Kyoto **UITP/K-1086** (1994).
- [5] F. Reines, H.S. Gurr, H.W. Sobel, *Phys. Rev. Lett.* **37** (1976) 315.
- [6] P. Vogel and J. Engel, *Phys. Rev. D* **39** (1989) 3378.
- [7] G.S. Vidyakin *et al.*, *JETP Letters (Rus.)* **55** (1992) 206.
- [8] A.I. Derbin *et al.*, *JETP Letters (Rus.)* **57**(1993) 768.
- [9] Z. Darakchieva *et al.*, *Phys. Lett. B* **615** (2005) 153.
- [10] H.T. Wong *et al.*, **hep-ex/0605006**.
- [11] D.W. Liu *et al.* [The Super-Kamiokande Collaboration], **hep-ex/0402015**.
- [12] J.F. Beacom and P. Vogel, **hep-ph/9907383**.
- [13] W. Grimus *et al.*, *Nucl. Phys. B* **648** (2003) 376; M.A. Tortola, **hep-ph/0401135**.
- [14] A.A. Vasenko *et al.*, *Prib. Techn. Exp. (Rus.)* **2** (1989) 56; *Mod. Phys. Lett. A* **5** (1990) 1299.
- [15] A.G. Beda, E.V. Demidova, A.S. Starostin, M.B. Voloshin, *Yad. Fiz. (Rus.)* **61** (1998) 72, [*Phys. At. Nucl.* **61** (1998) 66].
- [16] C.E. Aalseth *et al.*, *Nucl. Phys. B (Proc. Suppl.)* **70** (1999) 236.
- [17] A.G. Beda *et al.*, *Yad. Fiz. (Rus.)* **67** (2004) 1973, [*Phys. At. Nucl. (Engl. transl.)* **67** (2004) 1948].
- [18] E. Garcia *et al.*, *Nucl. Phys. B (Proc. Suppl.)* **28A** (1992) 286.
- [19] L.N. Bogdanova *et al.*, *Yad. Fiz. (Rus.)* **69** (2006) 1.
- [20] G.P. Škoro *et al.*, *Nucl. Instr. and Meth. A* **316** (1992) 333; R. Wordel *et al.*, *Nucl. Instr. and Meth. A* **369** (1996) 557.
- [21] V.I. Kopeikin, *Yad. Fiz. (Rus.)* **66** (2003) 500 [*Phys. of At. Nucl. (Engl. transl.)* **66** (2003) 472].
- [22] V.I. Kopeikin, *Yad. Fiz. (Sov.)* **32** (1980) 62.
- [23] P. Vogel *et al.*, *Phys. Rev. C* **24** (1981) 1543.
- [24] V. Kopeikin, L. Mikaelyan, V. Sinev, preprint "Kurchatov Institute" **IAE-6038/2** (1997).
- [25] A.M. Bakalyarov, V.I. Kopeikin, L.A. Mikaelyan, *Yad. Fiz. (Rus.)* **59** (1996) 1225 [*Phys. of At. Nucl. (Engl. transl.)* **59** (1996) 1157]; V.I. Kopeikin, L.A. Mikaelyan, V.V. Sinev, *Yad. Fiz. (Rus.)* **60** (1997) 230 [*Phys. of At. Nucl. (Engl. transl.)* **60** (1997) 172].
- [26] F.P. Larkins, *At. Data and Nucl. Data Tables* **20** (1977) 311.
- [27] V.I. Kopeikin *et al.*, *Yad. Fiz. (Rus.)* **61** (1998) 2032 [*Phys. of At. Nucl.*, **61** (1998) 1859]; S. Fayans, L. Mikaelyan, V. Sinev, *Yad. Fiz. (Rus.)* **64** (2001) 1.
- [28] L.A. Mikaelyan *Yad. Fiz. (Rus.)* **65** (2002) 1206.
- [29] Particle Data Group, *J. Phys. G* **33** (2006) 1.